

RSC Advances



This is an *Accepted Manuscript*, which has been through the Royal Society of Chemistry peer review process and has been accepted for publication.

Accepted Manuscripts are published online shortly after acceptance, before technical editing, formatting and proof reading. Using this free service, authors can make their results available to the community, in citable form, before we publish the edited article. This *Accepted Manuscript* will be replaced by the edited, formatted and paginated article as soon as this is available.

You can find more information about *Accepted Manuscripts* in the [Information for Authors](#).

Please note that technical editing may introduce minor changes to the text and/or graphics, which may alter content. The journal's standard [Terms & Conditions](#) and the [Ethical guidelines](#) still apply. In no event shall the Royal Society of Chemistry be held responsible for any errors or omissions in this *Accepted Manuscript* or any consequences arising from the use of any information it contains.

ARTICLE

Synthesis and characterization of $\text{Cu}_2\text{ZnSnS}_4$ thin films by the sulfurization of co-electrodeposited Cu-Zn-Sn-S precursor layers for solar cell applications

Cite this: DOI: 10.1039/x0xx00000x

Received 00th January 2012,
Accepted 00th January 2012

DOI: 10.1039/x0xx00000x

www.rsc.org/

Jiahua Tao^a, Junfeng Liu^a, Jun He^a, Kezhi Zhang^a, Jinchun Jiang^b, Lin Sun^{*a}, Pingxiong Yang^a, Junhao Chu^{a, b}

$\text{Cu}_2\text{ZnSnS}_4$ (CZTS) absorbers have been successfully deposited on tin-doped indium oxide coated glass (ITO/glass) substrates by sulfurization process of co-electrodeposited Cu-Zn-Sn-S precursor thin films at various annealing temperatures ranging from 500 to 580 °C for 30 min in the atmosphere of Ar/H₂S (6.5%). The effects of sulfurization temperature on the structure, morphology, composition and optical property of CZTS thin films have been investigated in details. XRD and Raman measurements reveal that the intensity of preferential orientation along the (1 1 2) direction becomes relatively more intense and sharp with increasing annealing temperature. The morphological and chemical composition studies indicate the formation of compact and homogenous CZTS thin films with Cu-poor and Zn-rich composition at a sulfurization temperature of 560 °C. And its band gap energy is around 1.50 eV. The AZO/i-ZnO/CdS/CZTS/ITO/glass thin-film solar cell is fabricated with the CZTS absorber layer grown at an optimized sulfurization temperature of 560 °C. It shows a power conversion efficiency of 1.98% for a 0.25 cm² area with $V_{oc} = 490$ mV, $J_{sc} = 9.69$ mA/cm² and FF = 40.03%.

1. Introduction

$\text{Cu}_2\text{ZnSnS}_4$ (CZTS) is one of the most promising photovoltaic materials as an alternative absorber layer for the development of low-cost and environmentally friendly thin film solar cells, which has a large absorption coefficient of over 10⁴ cm⁻¹ with a suitable direct band gap of about 1.5 eV.¹ Furthermore, theoretical power conversion efficiency of CZTS-based solar cells is estimated about 30%.² In 1988, Ito and Nakazawa first reported the photovoltaic effect of a CZTS thin film deposited by sputtering.³ Since then, various processing techniques have been reported to fabricate CZTS absorber layers including thermal evaporation,^{4, 5} sputtering,⁶⁻⁸ pulsed laser deposition,^{9,11} hybrid sputtering,¹² solution process,¹³ sol-gel deposition,^{14, 15} spray pyrolysis deposition¹⁶ and electrodeposition.¹⁷⁻²² Notably, vacuum-based deposition methods have relatively high production cost, so alternative low-cost and high throughput nonvacuum-based processes have been investigated and developed for the fabrication of CZTS absorber layers of high efficiency solar cells.^{14, 18, 22-24}

Among the above-mentioned nonvacuum methods, the electrodeposition is considered to be a viable alternative technique to obtain low-cost CZTS precursor films. Generally there are two different approaches for the electrodeposition of CZTS precursor films: (i) stacked elemental layer, and (ii) co-electrodeposited layer. Current issue for stacked precursor is the morphology of Sn precursor was very rough compared to the other elemental precursors. In addition, the poor morphology of CZTS is due to non-uniform nucleation of Zn precursor. Hence co-electrodeposition approach of CZTS precursors is preferred. Scragg *et al.* reported CZTS-based solar cells exhibiting 3.2% conversion efficiency via

stacked elemental layer in the order of Cu/Sn/Cu/Zn followed by sulfurization at 575 °C for 2 h in the atmosphere of H₂S.²² Ennaoui *et al.* also reported the fabrication of CZTS absorber layer for thin film solar cell with 3.4% conversion efficiency using co-electrodeposition of Cu-Zn-Sn precursors deposited followed by sulfurization in H₂S atmosphere at 550 °C for 2 h.²⁵ A key drawback of these methods used in the previous literature is the long sulfurization duration compared with our short annealing process (~30min) required for rapid growth of homogenous CZTS thin films. In addition, the phase of CZTS easily deteriorates during the long time annealing process, which gives rise to Sn loss by the decomposition into volatile SnS.²⁶ As a powerful annealing technique, rapid thermal processing has several advantages, including short cycle time for reaction, reduced thermal exposure and more flexibility, over the use of a conventional furnace in terms of temperature uniformity. Therefore, these factors motivate us to explore optimizing RTP process to grow homogeneous and densely packed morphology for CZTS absorber layers fabricated by co-electrodeposition. Up to date, the reported highest efficiency based on the electrodeposition has achieved 7.3% for CZTS solar cells fabricated by post-sulfurization of electrodeposited metal stacked layers at 585 °C for 12 min.²³ Current issue for metal stacked precursor is the morphology of Sn precursor is very rough compared to the other elemental precursors. In addition, the poor morphology of CZTS is due to non-uniform nucleation of Zn precursor.²² In comparison with the stacked elemental approach, co-electrodeposition approach has not been thoroughly investigated even though the simply fabrication process of the precursor is one of its significant advantages.

Generally, molybdenum (Mo) coated glass substrates are used for thin film solar cells in these reported literatures.²²⁻²⁵ So far, there are still few reports on the electrodeposition technology in the fabrication of CZTS-based solar cells for top tandem and bifacial devices using ITO as a back contact, which propels us to research the photovoltaic performance of CZTS thin film solar cells directly deposited on ITO/glass substrates. In this study, we have investigated the fabrication of CZTS precursor films deposited on ITO/glass substrates by co-electrodeposition followed by sulfurization process. The significant influence of the annealing temperature on the structure, morphology, composition and optical properties of CZTS thin films has been studied. It is observed that CZTS absorber layers exhibit closely packed grains and the best surface morphology at a sulfurization of 560 °C for 30 min.

2. Experimental

The Cu-Zn-Sn-S precursor thin films were deposited successively on ITO/glass substrates by using a three-electrode system with a silver/silver chloride (Ag/AgCl) as the reference electrode, a platinum (Pt) foil as the counter electrode and 230 nm ITO/glass substrates (20×25×1.1 mm², ITO thin films with $R_S=10\sim15 \Omega/\square$) as the working electrodes under potentiostatic control mode using a CHI660D electrochemical workstation (CH Instrument, USA). All raw chemicals are of analytical reagent grade (supplied by Sinopharm Chemical Reagent Co. Ltd., China). In order to get the close oxidation-reduction potential and a stable pH value, potassium tartrate (C₄H₄O₆K₂·1/2H₂O) and sodium citrate (Na₃C₆H₅O₇) in certain concentration were added in the electrolyte to mainly act as complexing agent and buffering agent. Before the electrodeposition, ITO/glass substrates were ultrasonically cleaned in acetone and then rinsed thoroughly with deionized water, and subsequently dried under flowing nitrogen gas. Cyclic voltammetry was conducted to determine the oxidation/reduction potentials of the electrolyte solution. The deposited Cu-Zn-Sn-S precursor thin films on ITO/glass substrates at -1.15 V (vs. Ag/AgCl) in an electrolyte solution containing CuSO₄·5H₂O (0.01 M), ZnSO₄·7H₂O (0.02 M), SnSO₄·2H₂O (0.02 M), C₄H₄O₆K₂·1/2H₂O (0.02 M), Na₃C₆H₅O₇ (0.02 M), and Na₂S₂O₃·5H₂O (0.01 M) at room temperature for 10 min without stirring. After the deposition, the samples were rinsed with deionized water and then dried under flowing nitrogen gas. The Cu-Zn-Sn-S precursor layers were loaded into a quartz container, which was inserted into a tube furnace. The rapid sulfurization annealing process was performed in the Ar/H₂S (6.5%) atmosphere with the pressure of 10 Torr and heated to the temperature range from 500 °C to 580 °C at a ramping rate of 50 °C min⁻¹, which was maintained for 30 min and then the system was cooled down naturally to room temperature. Sheet resistance of ITO films taken from ITO back contact after mechanical removal of the precursor and the CZTS thin films deposited on ITO/glass substrates. The completed CZTS solar cell device with the commonly employed structure of AZO/i-ZnO/CdS/CZTS/ITO/glass were prepared in the present study. The CdS buffer layer with 60 nm thickness was grown by chemical bath deposition from an aqueous solution of CdSO₄ (1.5 mM), thiourea (75 mM) and ammonia (1.8 M). Then undoped zinc oxide of about 50 nm thickness and Al-doped ZnO (AZO) of approximately 600 nm thickness were deposited by radio-frequency (RF)-magnetron sputtering. Finally, a mechanical scribing step was performed to define the cell area to 0.25 cm².

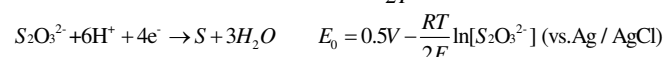
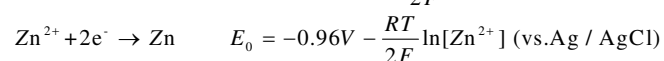
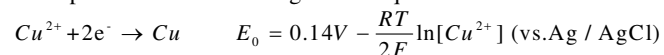
The structural properties of as-deposited and annealed films were determined by X-ray diffraction (XRD) using a BrukerD8 diffractometer (D/MAX-2200, Rigaku Co.) with Cu K α radiation ($\lambda=1.5406 \text{ \AA}$). Raman measurements were performed using a micro-

Raman spectrometer (Jobin Yvon Lab RAM HR 800UV Micro PL). For excitation, an Ar⁺ laser with 488 nm wavelength was used. The morphology and chemical composition were measured using a PhilipsS360 scanning electron microscope (SEM) attached to an energy-dispersive X-ray spectroscope (EDS). The element component of its average between two points in 2×2 μm^2 area was determined. The optical properties of the films grown on ITO/glass substrates were recorded using an ultraviolet-visible-near-infrared (Perkin Elmer Lambda 950) double-beam spectrophotometer. Sheet resistance was measured by four-point probe (NI PX1e-1062Q). Current density-voltage (*I-V*) characteristics of the CZTS solar cells were measured using a Photo Emission Tech solar simulator under AM 1.5 (100mW cm⁻²) illumination.

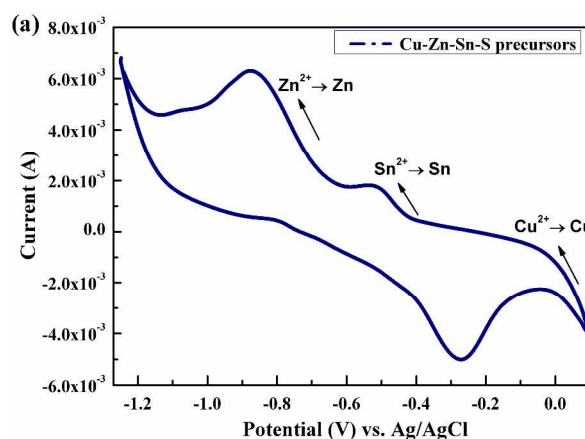
3. Results and discussion

3.1 Electrolyte formula and co-electrodeposition parameters of Cu-Zn-Sn-S precursor films

The conditions of co-electrodeposition of Cu-Zn-Sn-S precursor layers are related to the individual electrochemical reactions which correspond with the following Nernst equations.²⁷



It is clear, from the above equations, that copper, zinc, tin and sulfur have the large difference in the standard reduction potentials. Reduction potential of zinc has a more negative than that of copper and tin. So it is more difficult to be co-electrodeposited from the electrolyte solution. In order to narrow down the potential gap among three elements, a certain amount of trisodium citrate was added to the electrolyte. It has been reported previously that the citrate anion and copper cation form complex compound, which induce the reduction potential of copper to the more negative potential. Cyclic voltammetry is a potentiodynamic electrochemical technique generally used to study the process taking place at the electrode-electrolyte interface through the use of advanced computational modeling and high performance computing.



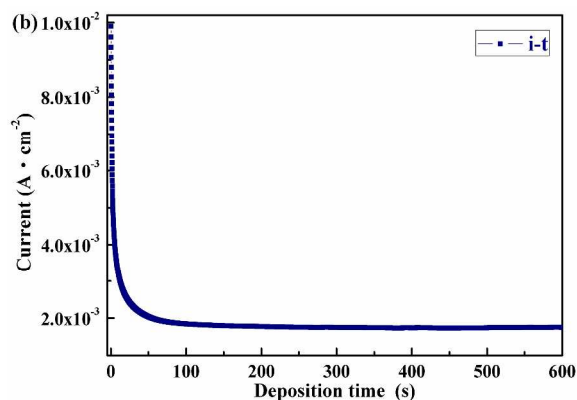


Fig. 1 (a) Cyclic voltammetry diagram of the electrolyte solution, scanned from 0.12 to -1.3 V at a rate of 10 mV s⁻¹. Arrows indicate scan directions. (b) Chronoamperograms during the electrodeposition with constant potential at -1.15 V (vs. Ag/AgCl) for 10 min.

The cyclic voltammetry measurement was carried out in the range from 0.12 to -1.3 V (vs. Ag/AgCl) at a scan rate of 10 mVs⁻¹ to investigate the growth parameters and optimize the co-electrodeposited potential in the same electrolyte solution. **Fig. 1(a)** shows reduction of Cu²⁺ and Sn²⁺ ions starts at 0.1 and -0.45 V (vs. Ag/AgCl) respectively, whereas Zn²⁺ can be reduced at about -0.7 V (vs. Ag/AgCl). In order to get exactly the desired content of Zn concomitantly with Cu and Sn by adjusting the ionic concentration in the electrolyte solution and the deposition potential. **Fig. 1(b)** displays the typical current density-time curve of Cu-Zn-Sn-S precursor films on ITO electrode at E_p = -1.15 V (vs. Ag/AgCl). As can be seen in the chronoamperogram (**Fig. 1(b)**), the current density curve abruptly decreases due to the successive diffusion of monomers from the bulk and reduction of more monomers on the ITO electrode surface, reaching the minimum. This period of time is called induction time.²⁸ Then the process reaches a stationary state called current plateau before nucleation and growth of the polymer begin, which is commonly observed for the electrodeposition controlled by convective mass-transfer.

3.2 Structure analysis

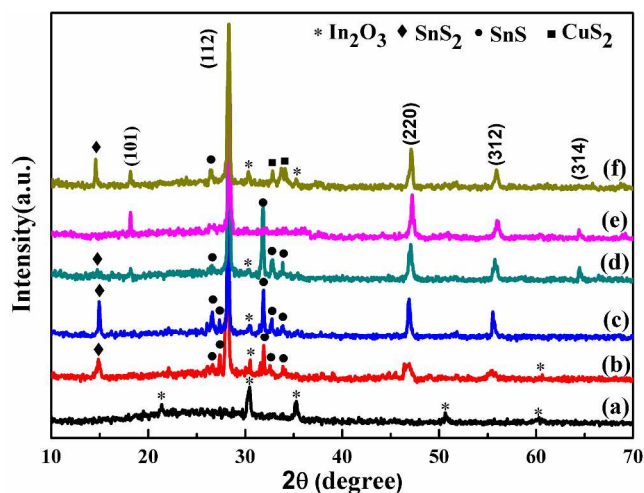


Fig. 2 XRD patterns of (a) CZTS-Precursor, (b) CZTS-500, (c) CZTS-520, (d) CZTS-540, (e) CZTS-560 and (f) CZTS-580.

Fig. 2 displays XRD patterns of the as-deposited and the samples annealed at various temperatures for 30 min in the atmosphere of Ar/H₂S. The as-deposited and annealed CZTS precursor films at 500, 520, 540, 560 and 580 °C are designated as CZTS-Precursor, CZTS-500, CZTS-520, CZTS-540, CZTS-560 and CZTS-580, respectively, where numbers represent various annealing temperatures. For the CZTS-Precursor (**Fig. 2(a)**) reveals some peaks only corresponding to ITO diffraction peaks of (2 1 1), (2 2 2), (4 0 0), and (4 4 0) planes indicating that the precursor is amorphous in nature.²⁹ The annealed films exhibit a polycrystalline kesterite CZTS crystal structure with major diffraction peaks towards (1 1 2), (2 0 0), (2 2 0), and (3 1 2) planes, which is confirmed using JCPDS card 23-0677. Moreover, the intensity of preferential orientation along the (1 1 2) plane becomes relatively more intense and sharp due to the enhancement in the crystallinity with increasing annealing temperature.²⁰ As shown in **Fig. 2(b)** and **Fig. 2(c)**, the XRD patterns of CZTS-500 and CZTS-520 have several reflections assigned to kesterite CZTS together with reflections of the SnS₂ (JCPDS 23-0677) and SnS (JCPDS 32-1361). The CZTS-540 shows in **Fig. 2(d)**, the minor peaks of SnS₂ disappear but there are some peaks from SnS besides those from CZTS, indicating the replacement of the SnS₂ phase with SnS during high temperature sulfurization process. In particular, when the sulfurization temperature was 560 °C, the XRD pattern of the CZTS-560 (**Fig. 2(e)**) is evident that there is no peaks related to the presence of binary and ternary compounds, which means that the film can be almost pure CZTS with better crystallinity. However, as further increase in annealing temperature, in CZTS-580 (**Fig. 2(f)**), secondary phases of Cu₂S (JCPDS no. 29-0578), SnS, SnS₂ and ZnS appear, as result of CZTS decomposition that occurs at temperature higher than 550 °C.^{30,31} Furthermore, the XRD results are needed to be confirmed by Raman spectra since CZTS, Cu₂SnS₃ and β-ZnS share similar crystal structures. For the annealed CZTS films deposited on ITO/glass substrates, the intensity of and the FWHM of (2 2 2) peak at 2θ=30.581° for ITO films become relatively weak and broad, respectively;²⁹ However, for the annealed CZTS films deposited on Mo/glass substrates, the intensity of and the FWHM of (1 1 0) peak at 2θ=40.504° peak for Mo films are still strong and sharp, in addition, MoS₂ phase is formed during the sulfurization process.^{8,14,32} This suggests that post-annealed process can reduce the crystalline quality of ITO thin films, leading to degradation of conducting performance. This result is well consistent with sheet resistance of ITO thin films (**Fig. 6**).

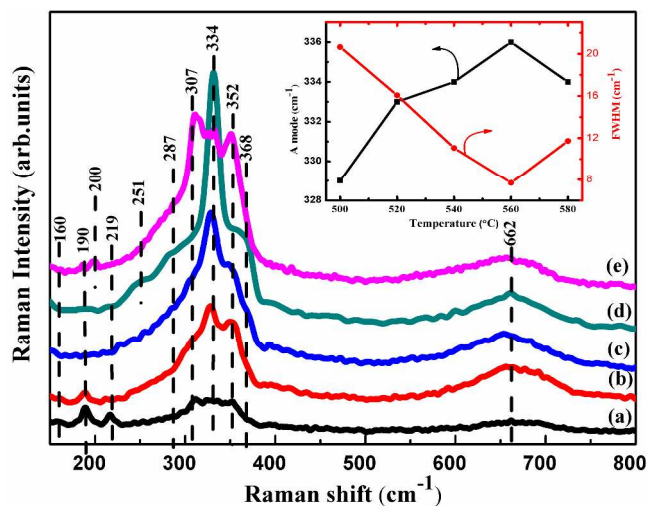


Fig. 3 Room temperature Raman spectra of (a) CZTS-500, (b)

CZTS-520, (c) CZTS-540, (d) CZTS-560 and (e) CZTS-580. Inset is the FWHM of CZTS films A_1 mode at around 334 cm^{-1} .

Fig. 3 presents the Raman spectra of these films measured at room temperature using the excitation laser wavelength of 488 nm . The dominant Raman peaks of these films are at $330\text{-}338\text{ cm}^{-1}$ range.^{6, 9} The small peaks at 662 cm^{-1} are the second-order Raman scattering peaks of these dominant peaks.⁷ Previous literatures have reported that the main Raman characteristic peaks of CZTS powders or films are near 338 cm^{-1} .⁹ Therefore, the Raman peak of these films are slightly broader and shifted towards low wave number direction with respect to those of the bulk crystal, which maybe implies the existence of internal stress in these films, which is not conducive to completely release the internal stress during the rapid cooling process.^{9, 10} The effect of annealing temperature can be better understood by comparing the width at half maximum (FWHM) values of Raman peaks. The variation FWHM of the A_1 mode at around 334 cm^{-1} with the change in the average size of CZTS particles shows that the main Raman peak becomes strong and narrow with increasing annealing temperature. In addition, FWHM of the Raman peaks are very broad, generally suggesting the poor crystallinity of thin films. Therefore, higher sulfurization temperatures are beneficial to the improvement of crystallinity for CZTS thin films. It has been observed from **Fig. 3(a)** and **Fig. 3(b)**, peaks at $160, 190$ and 219 cm^{-1} are assignable to SnS and a weak peak at 352 cm^{-1} may be convoluted peak of CZTS and ZnS, along with a moderate peak due to ITO at 307 cm^{-1} . But SnS_2 peaks observed in the XRD pattern is not appeared in Raman spectra SnS_2 peak 200 cm^{-1} , possibly due to only a small amount of SnS_2 impurity phase. When the temperature rises to $540\text{ }^\circ\text{C}$, SnS peak disappears, a weaker peak at 352 cm^{-1} is attributed to ZnS, and CZTS peak becomes stronger. When the temperature increases further to $560\text{ }^\circ\text{C}$, the Raman spectra of the CZTS-560 (**Fig. 3(d)**) displays peaks positioned at $251, 287, 334$ and 368 cm^{-1} , corresponding to CZTS.³² The CZTS-580 (**Fig. 3(e)**) reveals an intense peak assignable to a SnS_2 at 200 cm^{-1} , a peak at 352 cm^{-1} attributed to ZnS, and a weak In_2O_3 peak at 307 cm^{-1} , which is entirely consistent with the XRD result. The secondary phase of CuS_2 peaks detected in the XRD pattern is not observed in Raman spectra CuS_2 peak at 475 cm^{-1} in its corresponding Raman spectrum, which is possibly due to the fact that Raman measurements were performed using a micro-Raman spectrometer (the detection area is only at micrometer scale) and it reflect the signal of micrometer-scale local area, whereas XRD (the detection area is at least centimeter scale) can give the total signal of samples. And CuS_2 is possibly not in the scope of local Raman detection.

3.3 Morphology and composition characterization

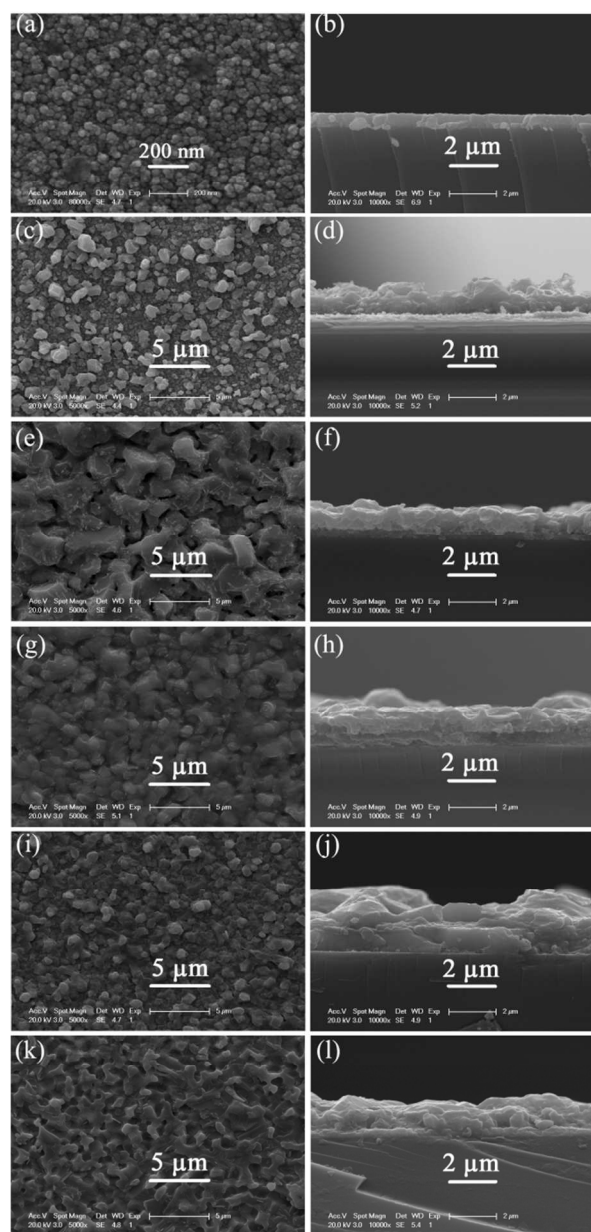


Fig. 4 Surface and cross-sectional SEM images of (a, b) CZTS-Precursor, (c, d) CZTS-500, (e, f) CZTS-520, (g, h) CZTS-540, (i, j) CZTS-560 and (k, l) CZTS-580.

Fig. 4 shows surface and cross-sectional SEM images of as-deposited precursor films and CZTS films annealed at different temperatures. The surface of CZTS-Precursor is a uniform and compact distribution of cauliflower-like nanoparticles with average crystal sizes of $50\text{-}100\text{ nm}$. Additionally, from the cross-section SEM (**Fig. 4(b)**), it can be seen that the precursor thin film is densely packed with thickness approximately 600 nm . These are no voids and crevices between the precursor thin film and ITO/glass substrate, indicating a strong adhesion. The surface SEM image of the CZTS-500 indicates that the film exhibits a rough surface containing micron-sized particles, as shown in **Fig. 4(c)**; the corresponding cross-section view shows a rough structure with a thickness of approximately $1\text{ }\mu\text{m}$ caused a substantial volume expansion which is around 1.5 times the original thickness of the precursor thin film (**Fig. 4(d)**). For CZTS-520 and CZTS-540 films, the disappearance

of the granular shape with micrometer-sized voids and crevices on the surface of the CZTS film, leads to forming a relatively uniform, smooth and compact films as evident from Fig. 4(e) and (g). Their cross-sectional images indicate the occurrence of growth accompanied by the formation of a double layer structure with grooved large grains at the top, and dense nanometric grains at the bottom near the back contact, as shown in Fig. 4(f) and (h); the thicknesses of the films are 1.45 and 1.85 μm , respectively. It demonstrates the annealing temperature not only improve the microstructure of CZTS films but also increase film thickness. When the annealing temperature is 560 $^{\circ}\text{C}$, the micron-sized and densely packed larger grains and void-free structure are observed (Fig. 4(i)). There is a homogeneous and densely-packed morphology for the CZTS-560 film, which could reduce the recombination rate of the photo-generated electrons and holes.³² The double layer structure existed in CZTS-520 and CZTS-540, becomes into one closely packed-grain layer which is desirable for yielding compact and faceted morphology with uniform surface, as seen in Fig 4(j). There are no voids and crevices at the interface between the film and the ITO/glass, indicating a fairly good adhesion of the film to the substrate. Although sulfurization at higher temperature of 580 $^{\circ}\text{C}$ results in further grain growth, the decomposition of CZTS thin film, the formation of voids and cracks become obvious, as shown in Fig. 4(k). Indeed, the film sulfurized at 580 $^{\circ}\text{C}$ is easily peeled off from the ITO/glass substrate. The film thickness is approximately 1.5 μm (Fig. 4(l)). It is thinner than that of CZTS-560 film annealed at lower temperature, due to the decomposition of CZTS thin films at higher temperature. For the annealed CZTS films deposited on Mo/glass substrates, the formation of MoS_2 interfacial layer at the CZTS/Mo interface is inevitable during sulfurization process,^{14, 23} which may facilitate an electrical quasi-Ohmic contact and improve the adhesion of CZTS to the Mo back contact. However, this leads to high series resistance and accordingly degrades the solar cell performance if the layer is not thin enough.⁵ For the annealed CZTS films deposited on ITO/glass substrates, the CZTS/ITO interface easily forms a good adhesion with a fairly good ohmic contact (Fig. 4). Thus, ITO/glass substrates can prevent the formation of MoS_2 layer and accordingly reduce the series resistance of the interface between CZTS and ITO. However, ITO itself contains high sheet resistance, leading to some degradation on device performance especially in J_{sc} and FF.

Table 1 Chemical composition and composition ratios of the precursor and sulfurized CZTS thin films.

Samples ID	Chemical composition (at. %)				Composition ratio		
	Cu	Zn	Sn	S	Cu/(Zn+Sn)	Zn/Sn	S/metal
CZTS-Precursor	40.80	24.94	17.60	16.66	0.96	1.42	0.20
CZTS-500	21.09	16.35	15.24	47.32	0.67	1.07	0.90
CZTS-520	21.32	15.58	14.39	48.71	0.71	1.08	0.95
CZTS-540	19.15	17.69	13.95	49.21	0.61	1.16	0.97
CZTS-560	19.67	16.36	13.02	50.95	0.67	1.26	1.04
CZTS-580	19.93	15.61	12.56	51.90	0.71	1.24	1.08

Table 1 presents the compositions of the Cu-Zn-Sn-S precursor (i.e. CZTS-Precursor) and the CZTS films sulfurized at various temperatures, determined by EDS measurements. The precursor is Cu-poor, S-poor and Zn-rich with composition ratios of Cu/(Zn+Sn) and Zn/Sn are 0.96 and 1.42. After sulfurization, the Cu and Sn contents in the CZTS films decrease with increasing annealing temperature. Moreover, the amount of sulfur and S/metal ratios also are gradually increase to about 50% and 1.00, indicating that sufficient sulfurization is achieved. It is beneficial to decrease the amounts of sulfur vacancies and improve the crystalline quality of

CZTS thin films.⁷ In addition, it is observed evidently that the ratios of Cu/(Zn+Sn) and Sn content decrease while Zn/Sn increases slightly in sulfurized thin films in comparison with the precursor (i.e. CZTS-Precursor), revealing the severe loss of Sn due to high volatility of tin sulfide during the sulfurization process.³³ The composition of the CZTS films are Cu/(Zn+Sn)=0.61~0.71 and Zn/Sn=1.07~1.26, which is lowly Cu-poor and seriously Zn-rich compared to the champion electroplated CZTS solar cell (with η =7.3%, Cu/(Zn+Sn)=0.78, Zn/Sn=1.35).²² This reveals that the amount of Cu in our CZTS films is lower than that of those reported for previous record devices.²²⁻²⁵ Further an optimization of the ratio of Cu/(Zn+Sn) in CZTS thin films could be approximately controlled by increasing the concentration of copper ions (ii) in the electrolyte solution and reducing the deposition potential.²⁷ In short, the compositions of CZTS thin films are strongly dependent on the sulfurization temperature as well as electrodeposition parameters.

3.4 Optical properties of CZTS thin films

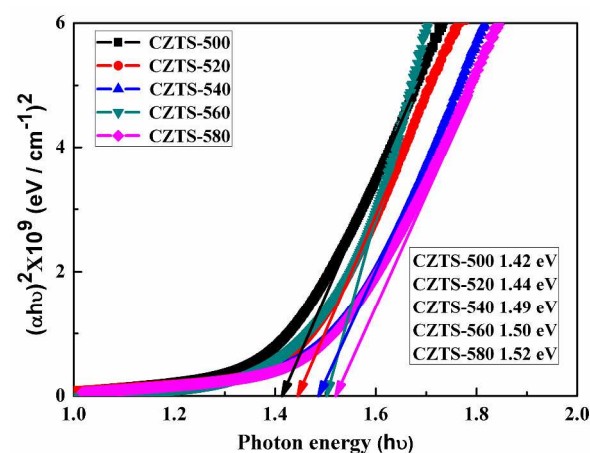


Fig. 5 Plot of $(\alpha h\nu)^2$ versus the photon energy ($h\nu$) for CZTS-500, CZTS-520, CZTS-540, CZTS-560 and CZTS-580.

The optical transmittance spectrum of the CZTS film annealed at various temperatures were measured for the determination of E_g . From the transmittance spectra, the absorption coefficient α was evaluated by equation $\alpha = -\ln(T)/t$, where T is the transmittance of the film and t is the film thickness. The band gap of the films is determined by extrapolating the linear region of the α^2 versus photon energy ($h\nu$) curve to the intercept of the $h\nu$ axis.^{7, 34} As shown in the Fig. 5, these determined E_g values of five CZTS films (i.e. CZTS-500 CZTS-520, CZTS-540, CZTS-560 and CZTS-580) are 1.42, 1.44, 1.49, 1.50, and 1.52 eV, respectively. E_g value of CZTS-560 is quite consistent with that of the reported experimental results^{6, 35} and E_g increases gradually with the increase in annealing temperature. It is possibly due to the fact that secondary phases such as SnS ($E_g=1.34$ eV) might exist in the CZTS films (i.e. CZTS-500 CZTS-520 and CZTS-540).³⁵ Moreover, the secondary phase SnS has been confirmed in the part of XRD and Raman measurements. The presence of SnS in the CZTS thin films is possibly responsible for the lesser E_g . Obviously, the optical band gap of CZTS-580 is much larger than those of all other thin films. This is due to the fact that secondary phase such as ZnS ($E_g=3.2$ eV) is much larger values of band gap.⁹ Actually, ZnS phase has been confirmed by Raman spectra of CZTS-580. As analyzed above XRD, Raman spectra, SEM, EDS, and optical analyses, the CZTS film grown at an optimized sulfurization temperature of 560 $^{\circ}\text{C}$ has better crystallinity, more homogeneous and compact surface morphology,

and more suitable band gap.

3.5 Sheet resistance of ITO thin films

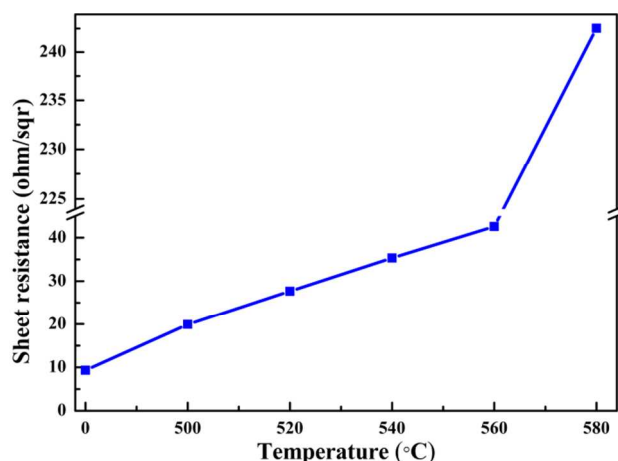


Fig. 6 Sheet resistance of ITO films after sulfuration treatment.

Fig. 6 shows sheet resistance (R_s) of ITO films obtained ITO back contact after mechanical removal of the precursor and the sulfurized CZTS films. R_s value measured by four-point probe almost linearly increases with the increase in sulfuration temperatures ranging from 500 to 560 °C. It is possibly due to the fact that H_2S gas can diffuse at the ITO/CZTS precursor interface. R_s value of the original ITO is ~ 9 ohm/sqr at room temperature. When the sulfuration temperature is 560 °C, R_s value of the ITO is ~ 43 ohm/sqr which is about 5 times the value of the original ITO due to increasing the sulfuration temperature. When the annealing temperature is up to 580 °C, R_s value of the ITO is 242 ohm/sqr which may be caused by over high sulfuration temperature.

3.6 Properties of CZTS thin film solar cells

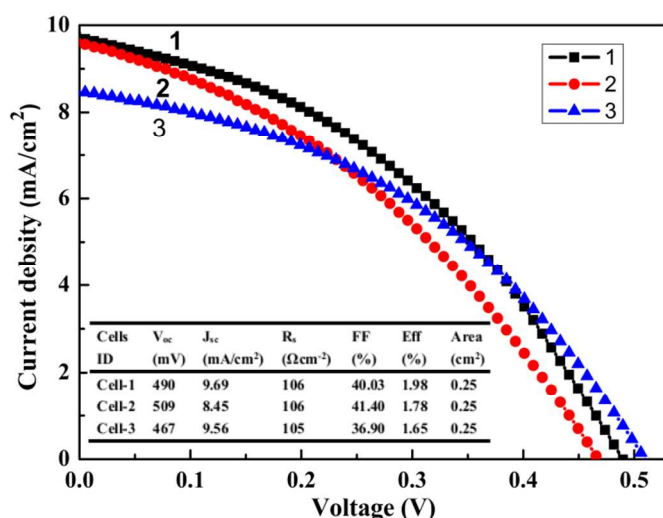


Fig. 7 Current-voltage characteristics of the solar cell fabricated with the CZTS-560/ITO.

Table 2 Photovoltaic parameters of reported conversion efficiencies for CZTS solar cells deposited on Mo/glass substrates processed by the electrodeposition.

Method	Sulfuration temperature and time	Eff (%)	V_{oc} (mV)	J_{sc} (mA/cm^2)	R_s (Ωcm^2)	R_{sh} (Ωcm^2)	FF (%)	Refs.
SEL	585 °C for 12 min	7.3	567	22.0	4.1	368	58.1	23
SEL	580 °C for 10 min	5.6	640	19.8	-	-	45.0	32
CEL	590 °C for 15 min	5.5	673	18.7	13.5	215.8	44.0	17
CEL	550 °C for 2 h	3.4	563	14.8	2.9	95.2	41.0	25
SEL	575 °C for 2 h	3.2	480	15.3	-	-	45.0	22
CEL	600 °C for 2 h	3.16	540	12.6	1.8	24.2	46.4	37
CEL	550 °C for 2 h	1.2	315	12.27	-	-	31.0	38
CEL	600 °C for 2 h	0.98	262	9.85	-	-	37.9	1
CEL	560 °C for 30 min	1.98	490	9.69	106	788	40.0	Our study

SEL, stacked elemental layer; CEL co-electrodeposited layer. Except for our using ITO/glass substrates.

The CZTS-560 thin films have been fabricated to photovoltaic devices with the structure of AZO/i-ZnO/CdS/CZTS/ITO/glass configuration. The previously reported device parameters for CZTS thin films deposited on Mo/glass substrates were listed in **table 2**, including our devices deposited on ITO/glass substrates. The CZTS solar cells with conversion efficiency of $> 5\%$ have been fabricated by the sulfuration of precursor films with sulfuration time for < 15 min at a temperature of > 580 °C. This suggests short sulfuration time and high sulfuration temperature were the critical sulfuration process of high efficiency CZTS/Mo solar cells. Cell-1, 2 and 3 in **Fig.7** are made of CZTS-560 film. Solar cell-1 gives a better conversion efficiency of 1.98% for a total area of $0.25 cm^2$ under simulated AM1.5 illumination, as shown in **Fig. 7**. Solar cell-2, 3 are other devices in the same sample which are close to the solar cell-1. They have conversion efficiencies of 1.78% and 1.65%, respectively, which indicates a relatively well-controlled composition distribution in the CZTS-560 absorber layer. Comparing the photovoltaic parameters of CZTS-560 device with that of higher CZTS devices reported in **Table 2**. The efficiency of 1.98% is much less than the reported the highest efficiency of the CZTS solar cell of 7.3%. The probable reasons are discussed and explained as follows: the series resistance of the solar cell with 1.98% is $106 \Omega cm^2$, while these were 4.1, 13.5, 2.9 and $1.8 \Omega cm^2$, respectively, for the reported solar cells with higher efficiencies in **Table 2**. The high series resistance of our solar cell leads to the reduced the efficiency and a substantial loss in fill factor because of the deterioration of the transport charge transfer and the recombination of charge carriers at the CdS/CZTS interface. From **Table 2**, it can be seen clearly that short circuit current density of $9.69 mA/cm^2$ is far less than those of other reported CZTS/Mo solar cells. So, there is much room for an improvement of circuit current density of our CZTS/ITO solar cell. In the present case, the high series resistance is possibly attributed to low electrical conductivity ITO electrode itself, especially after sulfuration process, as shown in **Fig. 6**. Moreover, the simulation of Merten *et al.* also identified that the series resistance is physically determined by the sheet resistance of the electrodes, especially that of the transparent electrode.³⁹ On the other hand, for our CZTS-560 sample, a small amount of the secondary phase (ZnS) may exist in the surface of the CZTS thin films due to the fact that the composition is a seriously Zn-rich (**Table 1**). Since ZnS with high series resistance is an inevitable question involved in the formation of CZTS thin films. It is also likely to contribute to the high series resistance of solar cell.

But the selective removal of the ZnS will become an effective method to improve device performance. ¹⁵ High shunt resistance ($R_{sh} = 788 \Omega \text{ cm}^{-2}$) may result from densely packed large grains in CZTS thin films for our CZTS/ITO solar cell. So, further improvement of the conversion efficiency could be achieved through the optimization of the composition of the electrolyte, electrodeposition parameters, annealing process and interface treatment.

4. Conclusions

We have fabricated CZTS thin films using cost-saving co-electrodeposition technique followed by annealing in the atmosphere of Ar/H₂S. The structure, morphology and optical properties of CZTS thin films depend mainly on sulfurization temperature. The crystalline quality of the kesterite CZTS thin films and the S content in the films can be obviously improved during the sulfurization process. The surface morphological studies indicate that the formation of large densely packed grains with compact and faceted morphology after annealing. At a sulfurization temperature of 560 °C, CZTS thin films are fully sulfurized with Cu-poor and Zn-rich composition, and its band gap is about 1.50 eV which is very close to the optimum value of absorber layers in CZTS-based solar cells. An AZO/i-ZnO/CdS/CZTS/ITO/glass solar cell with about 2% conversion efficiency has been obtained using the CZTS absorber sulfurized at 560 °C.

Acknowledgements

The authors are grateful to the help of Professor Zhigao Hu group in Raman scattering spectra. We also thank Yuchen Dong, Weijun Wang, Xiankuan Meng and Jun Zhang, for helpful discussions. This project was financed by the National Science Foundation of China (61106064) and the Science and Technology Commission of Shanghai Project (Grant No. 11ZR1411400, 10JC1404600).

Notes and references

^a Key Laboratory of Polar Materials and Devices, Ministry of Education, Department of Electronic Engineering, East China Normal University, 500 Dongchuan Road, Shanghai 200241, China. Tel.: +86 21 54345157; fax: +86 21 54345119. E-mail address: lsun@ee.ecnu.edu.cn (L. Sun).

^b Shanghai Center for Photovoltaics, Shanghai 201201, China

- [1] H. Araki, Y. Kubo, A. Mikaduki, K. Jimbo, W. S. Maw, H. Katagiri, M. Yamazaki, K. Oishi, A. Takeuchi, *Sol. Energy Mater. Sol. Cells* 93 (2009) 996-999.
- [2] W. Shockley, H. J. Queisser, *J. Appl. Phys* 32 (1961) 510-519.
- [3] K. Ito, T. Nakazawa, *Jpn. J. Appl. Phys* 27 (1988) 2094-2097.
- [4] K. Wang, O. Gunawan, T. Todorov, B. Shin, S. J. Chey, N. A. Bojarczuk, D. Mitzi, S. Guha, *App. Phys. Lett* 97 (2010) 143508-143510.
- [5] B. Shin, N. A. Bojarczuk, S. Guha, *Appl. Phys. Lett* 102 (2013) 091907-1-4.
- [6] F. Jiang, H. L. Shen, *RSC Adv* 3 (2013) 23474-23481.
- [7] R. B. V. Chalapathy, G. S. Jung, B. T. Ahn, *Sol. Energy Mater. Sol. Cells* 95 (2011) 3216-3221.
- [8] P. A. Fernandes, P. M. P. Salomé, A. F. Sartori, J. Malaquias, A. F. da Cunha, Björn-Arvid Schubert, J. C. González, G. M. Ribeiro, *Sol. Energy Mater. Sol. Cells* 115 (2013) 157-165.
- [9] L. Sun, J. He, H. Kong, F. Yue, P. Yang, J. Chu, *Sol. Energy Mater. Sol. Cells* 95 (2011) 2907-2913.
- [10] J. He, L. Sun, N. Ding, H. Kong, S. Zuo, S. Chen, Y. Chen, P. Yang, J. Chu, *J. Alloys Compd* 529 (2012) 34-37.
- [11] K. Moriya, K. Tanaka, H. Uchiki, *Jpn. J. Appl. Phys* 46 (2007) 5780-5781.
- [12] T. Tanaka, T. Nagatomo, D. Kawasaki, M. Nishio, Q. Guo, A. Wakahara, A. Yoshida, H. Ogawa, *J. Phys. Chem. Solids* 66 (2005) 1978-1981.
- [13] T. K. Todorov, J. Tang, S. Bag, O. Gunawan, T. Gokmen, Y. Zhu, D. B. Mitzi, *Adv. Energy Mater* 3 (2013) 34-38.
- [14] F. Y. Liu, K. W. Sun, W. Li, C. Yan, H. T. Cui, L. X. Jiang, X. J. Hao, M. A. Green, *Appl. Phys. Lett* 104 (2014) 051105-1-5.
- [15] Z. H. Su, K. W. Sun, Z. L. Han, H. T. Cui, F. Y. Liu, Y. Q. Lai, J. Li, X. J. Hao, Y. X. Liu, M. A. Green, *J. Mater. Chem. A* 2 (2014) 500-509.
- [16] Y. B. K. Kumar, G. S. Babu, P. U. Bhaskar, V. S. Raja, *Sol. Energy Mater. Sol. Cells* 93 (2009) 1230-1237.
- [17] J. Ge, J. C. Jiang, P. X. Yang, C. Peng, Z. P. Huang, S. H. Zuo, L. H. Yang, J. H. Chu, *Sol. Energy Mater. Sol. Cells* 125 (2014) 20-26.
- [18] S. N. Park, S. J. Sung, D. H. Son, D. H. Kim, M. Gansukh, H. Cheong, J. K. Kang, *RSC Adv* 4 (2014) 9118-9125.
- [19] K. Kornhuber, J. Kavalakatt, X. Z. Lin, A. Ennaoui, M. Lux-Steiner, *RSC Adv* 3 (2013) 5845-5850.
- [20] S. M. Pawar, B. S. Pawar, A. V. Moholkar, D. S. Choi, J. H. Yun, J. H. Moon, S. S. Kolekar, J. H. Kim, *Electrochim. Acta* 55 (2010) 4057-4061.
- [21] J. J. Scragg, P. J. Dale, L. M. Peter, *Thin Solid Films* 517 (2009) 2481-2484.
- [22] J. J. Scragg, D. M. Berg, P. J. Dale, *J. Electroanalytical Chem* 646 (2010) 52-59.
- [23] S. Ahmed, K. B. Reuter, O. Gunawan, L. Guo, L. T. Romankiw, H. Deligianni, *Adv. Energy Mater* 2 (2012) 253-259.
- [24] T. K. Todorov, J. Tang, S. Bag, O. Gunawan, T. Gokmen, Y. Zhu, D. B. Mitzi, *Adv. Energy Mater* 3 (2013) 34-38.
- [25] A. Ennaoui, M. Lux-steiner, A. Weber, D. Abou-Ras, I. Kotschau, H. W. Schock, R. Schurr, A. Holzing, S. Jost, R. Hock, J. Schulze, A. Kirbs, *Thin Solid Films* 517 (2009) 2511-2514.
- [26] A. Redinger, D. M. Berg, P. J. Dale, S. Siebentritt, *J. Am. Chem. Soc* 133 (2011) 3320-3323.
- [27] W. Septina, S. Ikeda, A. Kyoraiseki, T. Harada, M. Matsumura, *Electrochim. Acta* 88 (2013) 436-442.
- [28] M. A. Rasoia, M. J. González-Tejera, I. Carrillo, E. S. de la Blanca, M. V. García, M. I. Redondo, *Thin Solid Films* 519 (2011) 2387-2392.
- [29] D. Raoufi, A. Kiasatpour, H. R. Fallah, A. S. H. Rozatian, *Appl. Surf. Sci* 253 (2007) 9085-9090.
- [30] A. Weber, R. Mainz, H. W. Schock, *J. Appl. Phys* 107 (2010) 013516-1-6.
- [31] S. Kahraman, S. Çetinkaya, M. Podlogar, S. Bernik, H. A. Çetinkara, H. S. Güder, *Ceram. Int* 39 (2013) 9285-9292.
- [32] Y. Lin, S. G. Ikeda, W. Septina, Y. Kawasaki, T. Harada, M. Matsumura, *Sol. Energy Mater. Sol. Cells* 120 (2014) 218-225.
- [33] A. Redinger, S. Siebentritt, *Appl. Phys. Lett* 97 (2010) 1-3.
- [34] R. A. Wibowo, W. S. Kim, E. S. Lee, B. Munir, K. H. Kim, *J. Phys. Chem. Solids* 68 (2007) 1908-1913.
- [35] G. H. Yue, D. L. Peng, P. X. Yan, L. S. Wang, W. Wang, X. H. Luo, *J. Alloys Compd* 468 (2009) 254-257.

- [36] M. X. Wu, X. Lin, A. Hagfeldt, T. L. Ma, *Angew. Chem* 123 (2011) 3582-3586.
- [37] H. Araki, Y. Kubo, K. Jimbo, W. S. Maw, H. Katagiri, M. Yamazaki, K. Oishi, A. Takeuchi, *Phys. Status Solidi C* 5 (2009) 1266-1268.
- [38] S. M. Pawar, B. S. Pawar, K. V. Gurav, D. W. Bae, S. H. Kwon, S. S. Kolekar, J. H. Kim, *Jpn. J. Appl. Phys* 51 (2012) 10NC27-1-4.
- [39] J. Merten, J. M. Asensi, C. Voz, A. V. Shah, R. Platz, J. Andreu, *IEEE Trans. Electr. Dev* 45 (1998) 423-429.